Analysis of the Large-Signal Characteristics of Power Heterojunction Bipolar Transistors Exhibiting Self-Heating Effects

Apostolos Samelis and Dimitris Pavlidis, *Fellow, IEEE*

***Abstract*— The large-signal microwave characteristics of AlGaAs/GaAs heterojunction bipolar transistors (HBT's) are modeled using the conventional Gummel–Poon-based bipolar junction transistor (BJT) model and extending it to include self-heating effects. The model is incorporated as a user-defined model in a commercial circuit simulator. The experimental microwave characteristics of HBT's are analyzed using the new model and harmonic balance techniques and the impact of self-heating effects on the device large-signal characteristics is investigated. Use of constant base voltage rather than constant current is more suitable for achieving maximum output power. Self-heating induced by RF drive is reduced under constant base current conditions. Increased thermal capacitance values result in gain enhancement at high power levels.**

***Index Terms*— Heterojunction bipolar transistors, large-signal modeling, thermal effects.**

I. Introduction

A MAJOR obstacle for the employment of heterojunction bipolar transistors (HBT's) in high-power, high-frequency applications is related to device self-heating effects. Such effects are well known to cause significant degradation of the device operational characteristics, like degradation of the device gain and thermal runaway. Thermal effects in HBT's have been studied using approaches based on Drift–Diffusion [1] as well as analytical physical models [2], [3]. Technological solutions that provide thermally stable HBT's have also been recently addressed [4]–[6].

Self-heating effects have been incorporated in an HBT large-signal model by many researchers. Examples of them are the models in [7], [8]. Physically based SPICE-compatible HBT large-signal models have also been developed. The model in [9] accounts for self-heating, carrier drift in the emitter, current dependent junction capacitances, and emitter-base effective barrier bias dependence. An Ebers–Moll HBT model was implemented in [10] using LIBRA's user-defined elements. Finally, [11], [12] proposed an HBT model that differs from the traditional Ebers–Moll or Gummel–Poon models and used it to analyze the microwave power characteristics of HBT's. To the authors' knowledge, none of the above Gummel–Poon or Ebers–Moll models has been used for the analysis of the device microwave large-signal characteristics when self-heating effects are present. The analysis of such characteristics consists of the prime objective of the work presented in this paper.

In this paper, the Gummel–Poon-based HBT model is extended by incorporating self-heating effects and temperature-dependent model parameters, such as saturation currents, current gain, junction capacitances, built-in voltages, and band-gap energies. The implementation of the new HBT large-signal model in HP-EESof/LIBRA is presented in Section II. Section III describes the device dc characterization and the model parameter extraction procedure. In Section IV, the large-signal model is employed in the analysis of the microwave power characteristics of AlGaAs/GaAs HBT's using harmonic balance techniques and is validated by means of load-pull measurements. Finally, the impact of self-heating on device bias for two different amplifier biasing schemes and the role of the thermal capacitance is discussed in Section V.

II. A Fully Temperature-Dependent HBT Large-Signal Model

The AlGaAs/GaAs HBT under testing had a large emitter area (300 μm^2) and was intended for power applications. A conventional design was used employing an abrupt emitter-base heterojunction, a 700-Å-thick base and a 1-μm-thick GaAs collector. Self-aligned technology was used for transistor fabrication. Similar to [8], the model described in this paper is complete, (i.e., includes temperature dependence for most parameters). Moreover, it is based on the SPICE2 model formulation [13] which served as the basis of the large-signal analysis presented here. It must be noted here that bipolar junction transfer (BJT) models in SPICE follow the Gummel–Poon formulation which does not account for thermionic emission and tunneling at the heterojunction interface [14]–[18]. Nevertheless, one can employ such models to describe HBT characteristics if the device under study exhibits exponential characteristics. In such a case, the macroscopic parameters of the Gummel–Poon model can be used to directly fit the measured dc characteristics.

To confirm that employment of the Gummel–Poon model is sufficient for modeling the dc characteristics of the device

Manuscript received July 26, 1996; revised December 24, 1996. This work was supported by ARO under Contract DAAL 03-92-G-0109.

D. Pavlidis is with the Department of Electrical Engineering and Computer Science, Solid State Electronics Laboratory, University of Michigan, Ann Arbor, MI 48109-2122 USA.

A. Samelis was with the Department of Electrical Engineering and Computer Science, Solid State Electronics Laboratory, University of Michigan, Ann Arbor, MI 48109-2122 USA. He is now with Rockwell Semiconductor Systems, Newbury Park, CA USA.

Publisher Item Identifier S 0018-9480(97)02543-X.

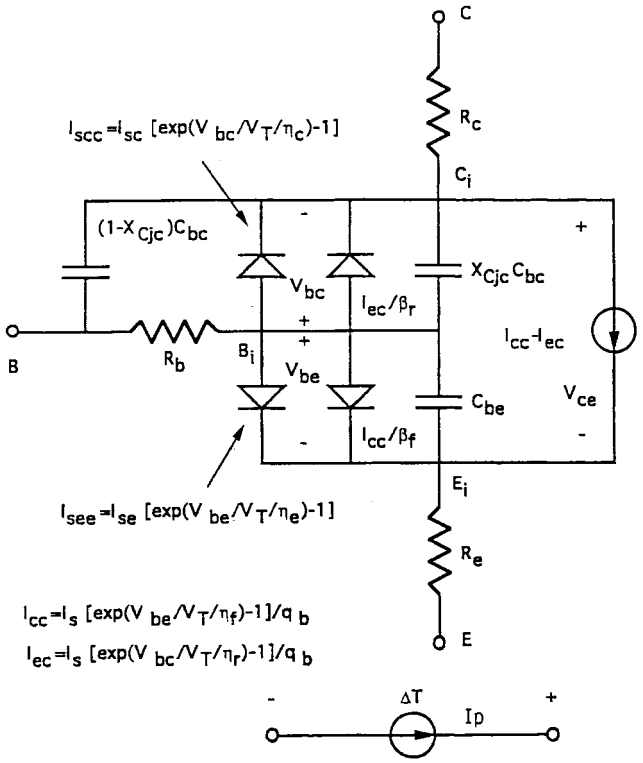

Fig. 1. Temperature dependent HBT large-signal model. I_p is the dc dissipated power which acts as a current source exciting the thermal sub-circuit.

studied in this work, the HBT I_C–$V_{\rm BE}$ characteristics were evaluated using the analytic procedure described in [14], [16] which accounts for thermionic emission and tunneling and is based on consideration of device design parameters such as layer thickness, dopings, etc. Simulation results based on the above models revealed an exponential I_C–$V_{\rm CE}$ dependence with ideality factor η_f and saturated current I_S values equal to 1.16 and 3.3×10^{-23} A, respectively. In the case of the experimentally obtained data, the corresponding fits resulted in $\eta_f = 1.31$ and $I_S = 3 \times 10^{-21}$ A. The authors have also derived such characteristics using a drift-diffusion model and found $I_S = 1.29 \times 10^{-25}$ A, $\eta_f \sim 1$. By comparing the I_C–$V_{\rm BE}$ characteristics obtained by the different techniques one sees that the measured data (described by the Gummel–Poon model parameters I_S and η_f) are closer to the exponential characteristics predicted by the thermionic emission/tunneling models. Moreover the measured data largely deviate from the drift-diffusion-based predictions. This implies suitability of the Gummel–Poon model in modeling HBT provided that its parameters obtained by empirical fittings result in exponential device characteristics.

The model was implemented as an user-defined *senior module* in the commercially available microwave circuit simulator, LIBRA, and is shown in Fig. 1. Its features include high injection effects, a bias-dependent forward transit time, and current crowding effects. A full temperature dependence for most of the model parameters like the zero-bias junction capacitances, the band gap, the built-in voltages, the device forward and reverse gains, and the saturation currents was considered. All model equations of the SPICE2 BJT model [13] were

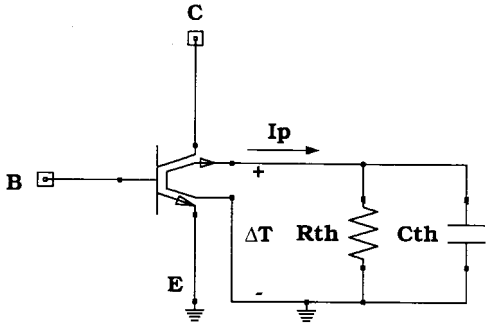

Fig. 2. HBT macromodel for power HBT.

rigorously reproduced, except the excess phase and the flicker noise parameters. A thermal sub-circuit was included and was coupled to the device so that HBT dc characteristics could be modified in the presence of thermal effects. The complete gain-temperature expression was employed as shown below:

$$\beta_f(T_2) = \beta_f(T_1)\left(\frac{T_2}{T_1}\right)^{X_{T\beta}} \exp\left[\frac{q\Delta E}{k}\left(\frac{1}{T_2}-\frac{1}{T_1}\right)\right] \quad (1)$$

where T_1 and T_2 are the substrate and device temperatures, respectively. Their difference, $\Delta T = T_2 - T_1$, results in a voltage difference across the thermal resistance, $R_{\rm th}$, as explained below. Equation (1) accounts for the variation of β_f with temperature by employing parameters reported in [3] (ΔE) and [13] $(X_{T\beta})$. As it turned out, only one parameter, namely ΔE, was sufficient for the analysis of thermal effects of the HBT under study. Therefore, the parameter $X_{T\beta}$ was assumed to be zero for the modeling purposes of this work.

The key point in the developed technique is the addition of two pins to the transistor, which permit connection of a current source to the HBT model in order to account for self-heating effects. The value of this current source, I_p, is equal to the power dissipated by the device and is given by

$$I_p = \left(\frac{I_{CC}}{\beta_f} + I_{\rm see}\right)V_{\rm be} + \left(\frac{I_{EC}}{\beta_r} + I_{\rm scc}\right)V_{bc} + (I_{CC} - I_{EC})V_{ce} + \frac{V_{BB_i}^2}{R_B} + \frac{V_{EE_i}^2}{R_E} + \frac{V_{CC_i}^2}{R_C}. \quad (2)$$

This current source excites the externally connected thermal sub-circuit which consists of a thermal resistance, $R_{\rm th}$, in parallel to a thermal capacitance, $C_{\rm th}$, as shown in Fig. 2. A thermal circuit can be represented by its electrical equivalent in which resistances (Ω), capacitances (F), voltages (V), and currents (A) correspond to thermal resistances (K/W), thermal capacitances (sW/K), temperatures (K), and power dissipation (W) of the thermal circuit, respectively [20]. Therefore, the voltage across this current source is equal in value to the temperature rise ΔT of the device. It should be noted that $R_{\rm th}$ depends, in general, on the device temperature and geometry. A more general dependence of $R_{\rm th}$ on its terminal temperature ΔT could be implemented as a separate user-defined SENIOR model linked together with the HBT model to LIBRA. The assumption of a constant $R_{\rm th}$ made in this work does not restrict use of the HBT model in conjunction to a more complex thermal sub-circuit since $R_{\rm th}$ is externally defined

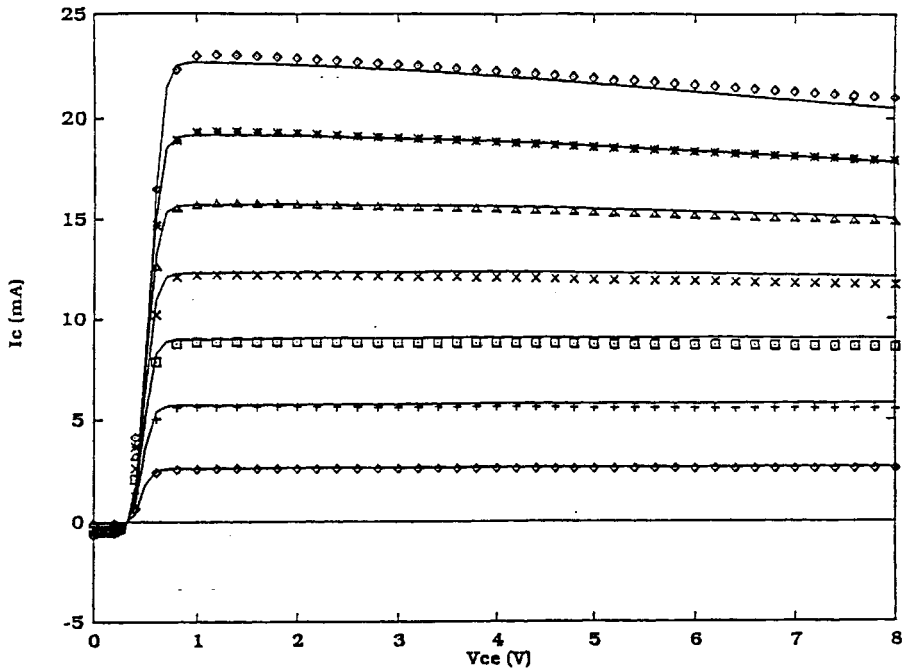

Fig. 3. Measured and simulated I_C–$V_{\rm CE}$ characteristics of power HBT. Bottom curve: $I_B = 0.1$ mA, Top curve: $I_B = 0.7$ mA, I_B-step $= 0.1$ mA.

with respect to the HBT as shown in Fig. 2. Other trends such as nonlinear temperature dependence of $R_{\rm th}$ could, for example, be used as dictated by theory or experiments [21], [22]. Negligence of the nonlinear $R_{\rm th}$ versus T dependence in the authors' model does not, however, have a major consequence on the reported results and assumption of a single constant for $R_{\rm th}$ is sufficient for the range of power levels dissipated by the device of this work.

Fig. 2 shows the macromodel used in the analysis of the power HBT. The thermal sub-circuit consists of $R_{\rm th}$ and $C_{\rm th}$. The HBT dc characteristics can consequently be modified when thermal effects are present by calculating the dc dissipated power, I_p, then calculating the temperature rise, ΔT, across the thermal sub-circuit and finally, use ΔT to evaluate the new device currents. The procedure is iterated until convergence of the device terminal characteristics is achieved. Moreover, the same circuit topology can be applied to individual HBT emitter fingers. In this way, one can account for the temperature rise due to heating by adjacent fingers and evaluate, therefore, the overall thermal characteristics of multifinger HBT's. This approach allows an extension of the standard HBT model available in LIBRA.

All node currents, charges, and their derivatives were defined in LIBRA. The latter not only involved voltage- but also temperature-dependent quantities. The linearized (small-signal) device model was developed, including temperature dependent small-signal current sources parallel to the base-emitter and base-collector conductances. Finally, the derivatives $\frac{dI_p}{dV_{\rm be}}$, $\frac{dI_p}{dV_{\rm bc}}$, and $\frac{dI_p}{dT}$ of the current source, I_p, of the thermal subcircuit were analytically calculated and added to the model. The inclusion of these derivatives in the model allowed better convergence of the harmonic balance algorithm.

The extended Ebers–Moll HBT large-signal model [19] was used as the reference for the device dc characterization. This included two leakage diodes between the base-emitter and base-collector contacts, respectively. The model parameters were empirically estimated using the data obtained from the device forward and reverse Gummel-plots and the I_C-$V_{\rm CE}$ characteristics.

TABLE I
GUMMEL–POON LARGE- SIGNAL MODEL PARAMETERS

Parameter	Value	Parameter	Value	Parameter	Value
I_S	$3.0158 \cdot 10^{-21}$ A	β_f	49	β_r	0.1
η_f	1.3122	η_r	1.0535	I_{SE}	$1.2388 \cdot 10^{-18}$ A
I_{SC}	$3.2799 \cdot 10^{-13}$	I_{KF}	0.0	I_{KR}	0.0
η_e	1.734	η_c	1.96	V_{AF}	0.0
V_{AR}	0.0	R_C	1.7768 Ω	R_E	4.5386 Ω
R_B	2 Ω	R_{BM}	2 Ω	I_{RB}	0.0
τ_f	4 ps	τ_r	1 ps	X_{TF}	0.0
V_{TF}	1.0	I_{TF}	0.0	C_{JE}	50 fF
V_{JE}	1.4 V	M_{JE}	0.5	C_{JC}	350 fF
V_{JC}	1.4 V	M_{JC}	0.5	X_{CJC}	1
FC	0.5	$X_{T\beta}$	0.0	X_{TI}	0
E_G	1.43 eV	T	300 K	α	0.0007
β	1108	ΔE	0.12 eV		

III. DEVICE CHARACTERIZATION AND MODEL PARAMETER ESTIMATION

The device model parameters were empirically extracted from dc data. The forward collector current parameters I_S and η_f were estimated by fitting of the forward Gummel-plot. The saturation current, I_{SE}, and ideality factor, η_e, of the base-emitter recombination diode were empirically specified from the measured I_B data. Similarly, the reverse operation related parameters, I_{SR}, η_r, I_{SC}, and η_c were determined from the reverse Gummel-plots.

The ideal forward common emitter gain, β_f, was adjusted to obtain a good fit of the I_C–$V_{\rm CE}$ characteristics of the device in the low-current active region where thermal effects are usually not significant. Finally, the reverse common-collector

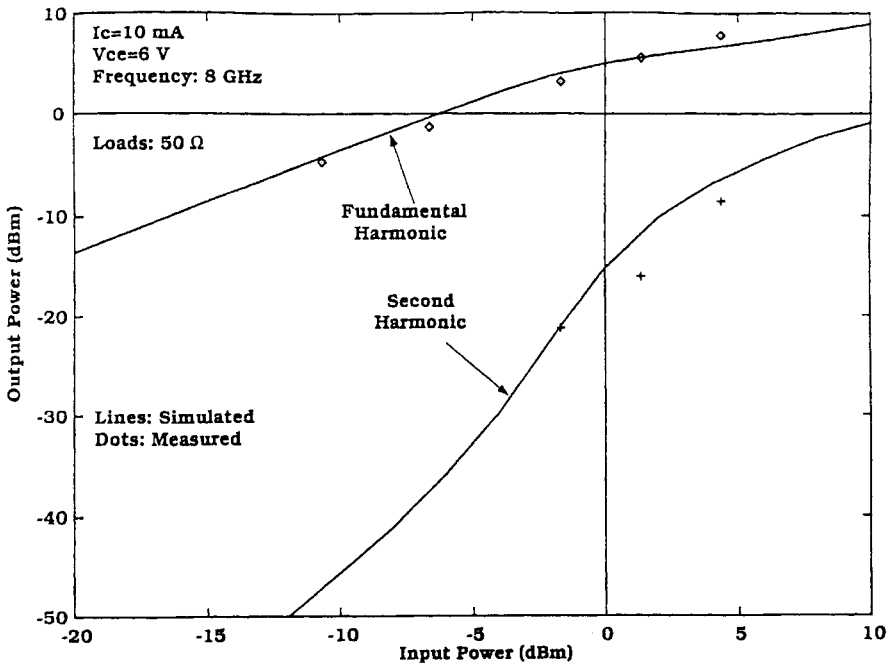

Fig. 4. Power characteristics of HBT operating under one-tone excitation.

current gain, β_r, was set to a value of 0.1 so that the I_E/β_r-base current component could be kept small. The latter was necessary since the emitter current was smaller than the total base current by more than two orders of magnitude.

Assuming that in the reverse operation mode the voltage drop across R_C due to I_E is much less significant than the voltage drop across R_B and R_C due to I_B, one can easily estimate the sum of the base and collector resistances from the reverse Gummel-plots. This sum was estimated to be $R_C + R_B = 3.77\ \Omega$ and the individual R_C, R_B values were assumed to be equal to 2 and 1.77 Ω, respectively. The emitter resistance was adjusted in order to obtain a good agreement in the I_C–$V_{\rm CE}$ characteristics between the measurements and the simulation in the saturation region of operation. A value of $R_E = 4.5\ \Omega$ was found appropriate for this purpose.

$R_{\rm th}$ and ΔE were chosen to be 150 K/W and 0.12 eV, respectively, so that a proper negative slope could be obtained for the I_C–$V_{\rm CE}$ characteristics. $R_{\rm th}$ can be obtained by measuring the device I_C–$V_{\rm BE}$ characteristics for different $V_{\rm CE}$ and substrate temperatures. One then plots, for a particular current, $V_{\rm BE}$ as a function of temperature and the device dissipated power as a function of $V_{\rm BE}$. Eliminating $V_{\rm BE}$, one finally obtains the dependence of temperature on dissipated power and, therefore, the thermal resistance of the HBT from the slope of the T versus power characteristics. The authors employed this technique for extracting $R_{\rm th}$ for AlGaAs/GaAs devices of similar design but different geometries and found good agreement with data reported by other groups [23]. Based on such considerations and by accounting for comparable geometries as, for example, reported in [5] the authors selected a thermal resistance value of $R_{\rm th}$ of 150 K/W for the HBT used in this work. ΔE is a constant representing the valence band discontinuity of the emitter–base interface [24]. For the $Al_xGa_{1-x}As$/GaAs system it is given by $\Delta E_v = 0.45x$ eV [25]. For the device under study $x = 0.35$ resulting in $\Delta E_v = 0.157$ eV. This value was used as a starting value for ΔE and was modified until best fit ($\Delta E = 0.12$ eV) was obtained between measured and modeled device dc characteristics. Finally, a thermal capacitance of $C_{\rm th} = 10^{-9}$ sW/K was assumed in device modeling giving a thermal time constant of 0.15 μs (i.e., significantly larger than the period of the applied RF-signal).

Table I shows all parameters used for the HBT macromodel in LIBRA. Fig. 3 shows the fitted and measured I_C-$V_{\rm CE}$ characteristics of the tested device. The key dc model parameters are also included in these figures. The results demonstrate an excellent agreement between experimental and simulated characteristics.

IV. Large-Signal Characterization and Modeling

The power characteristics of the device were measured using electromechanical tuners by Focus Microwaves, Inc. The bias operating conditions were set at $I_C = 10$ mA and $V_{\rm CE} = 6$ V and the excitation frequencies were 8 GHz (one-tone excitation) and 8 and 8.0001 GHz (two-tone excitation). The nonlinear products were measured using a Tektronix 2755P spectrum analyzer. Measurements taken under 50-Ω loading conditions were used in the analysis which follows.

The capacitive components of the HBT model were calculated using "cold" S-parameter measurements, (i.e., measurements under $I_B = 0$) and variable $V_{\rm CE}$ conditions as previously described by the authors [26]. The parasitic pad capacitances at the input and output of the device were extracted from these measurements and were both determined to be $C_{p1} = C_{p2} = 166$ fF. The base–collector capacitance, $C_{\rm BC}$ was analytically calculated from bias dependent S-

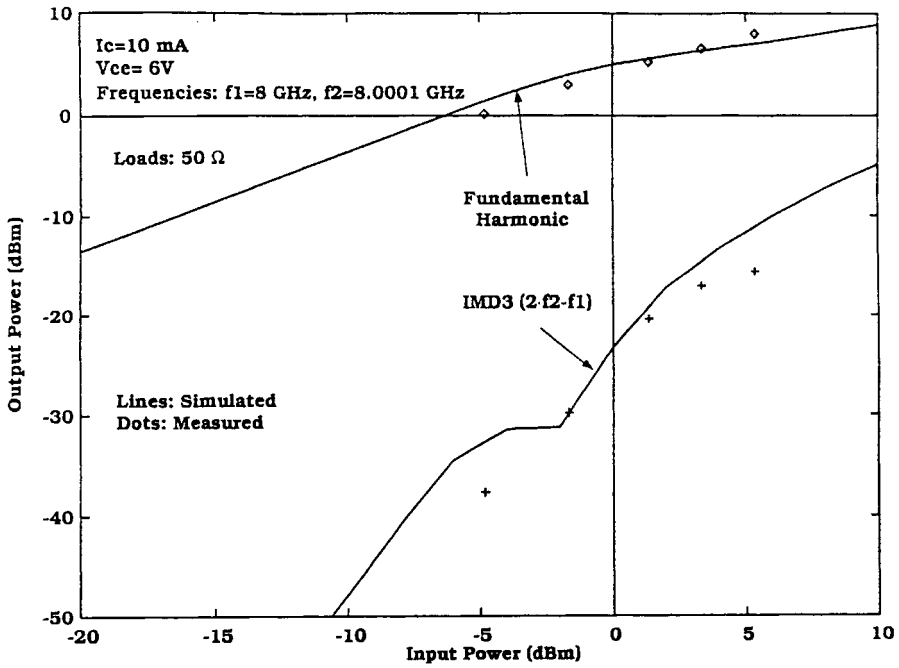

Fig. 5. Power characteristics of HBT operating under two-tone excitation.

parameter data [27]. Its zero-bias value was found to be $C_{jc} = 350$ fF. Furthermore, the forward transit time was chosen as $\tau_f = 4$ ps and the zero-bias emitter junction capacitance was chosen as $C_{je} = 50$ fF.

The microwave power characteristics of the HBT were analyzed under single- and double-tone excitation using the large-signal model presented above in conjunction with LIBRA's harmonic balance simulator. Five harmonics were used to assist convergence of the algorithm.

Fig. 4 shows the power of the fundamental and second harmonics generated by the device under one-tone excitation as a function of the available input power of the RF-excitation $P_{\rm in}$. Fig. 5 shows the power of the fundamental and the third-order intermodulation (IMD3) components generated under two-tone excitation conditions. Good agreement between the measured and simulated data is shown by the results of both figures and support the validity of the model.

V. Investigation of Impact of Self-Heating on Device Gain, Bias, and Efficiency

Using the developed HBT large-signal model, one can study the impact of large-signal excitation on the device large-signal characteristics such as gain, self-heating, and power-added efficiency. The HBT was terminated with a complex output load which consisted of an 1-nH inductor in parallel to a 50-Ω resistor. The device large-signal performance was investigated under various base bias conditions. Two different dc bias schemes were considered for this purpose. The first employed a constant base current while the second employed a constant voltage ($V_{\rm BE} = 1.4$ V) across the base–emitter junction. Both used a collector bias of $V_{\rm CE} = 6$ V.

Fig. 6(a) shows the dependence of the gain and the power-added efficiency (PAE) on available input power for the two bias schemes. Good agreement is observed for the gain and PAE values as a function of $P_{\rm in}$ under constant I_B ($I_B = 0.34$ mA) as shown by the experimental data which are repeated for comparison. One observes a PAE improvement over the entire range of power levels when constant $V_{\rm BE}$ is used. At low power levels the collector current is lower under constant $V_{\rm BE}$ bias. Self-bias and thus I_C, is low when constant $V_{\rm BE}$ bias is used resulting in lower gain in this case. Furthermore, the gain under constant I_B conditions shows flat characteristics followed by a region of compression while under constant $V_{\rm BE}$ bias a slight gain expansion is observed.

Self-heating effects are enhanced in case of HBT's with larger $R_{\rm th}$ values. By employing an $R_{\rm th}$ value of 500 K/W one obtains the characteristics shown in Fig. 6(b). Here, a higher base current of $I_B = 1.4$ mA was used for the constant I_B simulation scheme. The overall trends resemble those shown in Fig. 6(a) where good agreement was demonstrated between experimental and theoretical results for $R_{\rm th} = 150$ K/W. The characteristics depicted in Fig. 6(a) and (b) can be understood by examining the dependence of I_C on available input power. These are shown in Fig. 7 for the case of an $R_{\rm th}$ value of 500 K/W; a high $R_{\rm th}$ permits, again, better demonstration of the occurring effects without any impact on the overall trends and conclusions. Use of a constant I_B forces I_C, which follows an approximate $I_C = \beta \cdot I_B$ dependence, to be less sensitive on input power. On the other hand, use of constant $V_{\rm BE}$ bias allows rectification of the base current flowing through the base-emitter junction. Fig. 6 also shows that self-bias effects of this type are much stronger under constant $V_{\rm BE}$ bias. The RF input excitation turns on the device in this case at high power levels causing a collector current increase by self-bias which is of the order of 60 mA; self-bias under constant I_B bias is only of the order of 5 mA. Current rectification by constant $V_{\rm BE}$

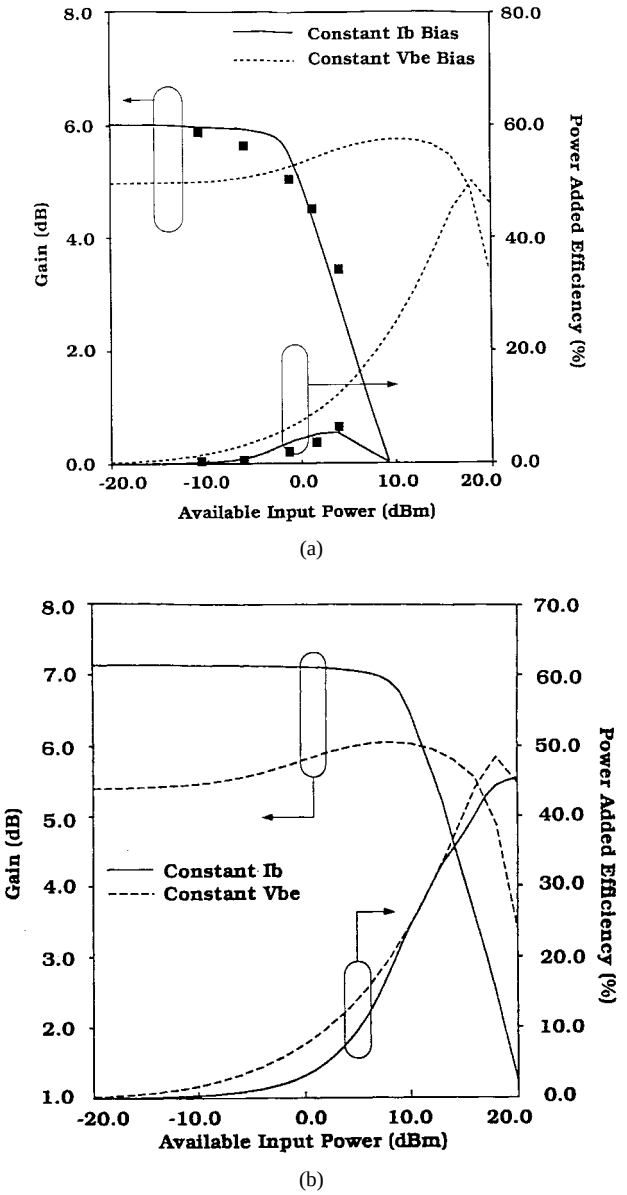

Fig. 6. Gain and PAE dependence on dc bias schemes and RF-excitation levels (a) ($R_{\rm th}$ = 150 K/W, I_B = 0.34 mA), (b) $R_{\rm th}$ = 500 K/W, I_B = 1.4 mA).

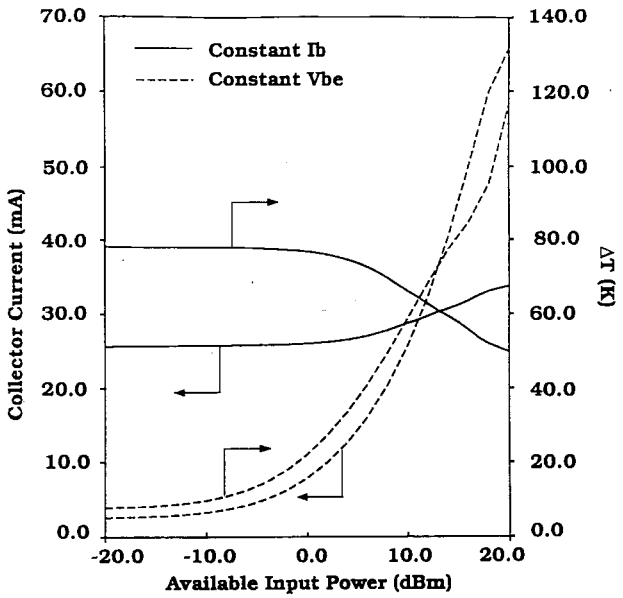

Fig. 7. Collector current and device temperature rise dependence on dc bias schemes and RF-excitation levels.

bias results consequently in higher I_B and, therefore, I_C values causing the gain to increase as the input power increases. This explains the gain enhancement characteristics shown in Fig. 6.

Fig. 7 also shows that the gain is compressed at high input power levels. This effect takes place earlier under constant I_B than constant $V_{\rm BE}$ conditions. As a result, although the gain and, thus, output power are smaller under constant $V_{\rm BE}$, they present superior characteristics at large input power levels due to delayed gain saturation. This is caused by the increase of I_C due to RF-excitation which reduces gain compression due to device cutoff under constant $V_{\rm BE}$ conditions. On the other hand, cutoff is more pronounced under constant I_B bias conditions and leads to stronger gain degradation. As a result, there is more than 2-dB gain advantage at input power levels of 20 dBm when the constant $V_{\rm BE}$ bias scheme is used. Finally, the gain compression manifested at high power levels for both bias schemes is attributed to HBT operation in both the saturation and cutoff regimes during the input signal RF-cycle.

The differences in self-heating are also significant among the two bias conditions. As Fig. 7 shows, the rise, ΔT of the junction temperature above 300 K follows the I_C characteristics and increases considerably with input power when constant $V_{\rm BE}$ is used. On the other hand, the device temperature drops with increasing RF-excitation if constant I_B is used for device bias. This behavior can be explained by considering that the HBT temperature is determined by the power dissipated by the device as already described by (2). The net power absorbed by the device can be written as

$$P_{\rm net} = P_{\rm dc} + P_{\rm in} - P_{\rm out} = P_{\rm dc}(1 - {\rm PAE}) \qquad (3)$$

where $P_{\rm dc}$, $P_{\rm in}$, and $P_{\rm out}$ are the dc dissipated power, the RF input power (absorbed by the device), and the RF output power (absorbed by the load). As one sees, $P_{\rm net}$ and thus ΔT will depend on two factors, namely, the PAE and $P_{\rm dc}$. The former is expected to increase with input power up to a certain power level and will consequently lead to a decrease of $P_{\rm net}$. $P_{\rm dc}$ on the other hand, is increased with input power due to the self-bias effects of I_C described earlier and causes an increase of $P_{\rm net}$ and, thus, device temperature. Both the above mechanisms are present under large-signal HBT operation and their particular characteristics for individual devices will determine whether the HBT temperature will increase or decrease with input power. Fig. 8 provides a better insight to the above effects by showing the device dissipated power $P_{\rm net}$ as a function of the available input power. As one observes, when a constant $V_{\rm BE}$ is used, $P_{\rm net}$ increases with input power causing the temperature to increase. On the contrary, when constant I_B is used, $P_{\rm net}$ decreases with input power causing the temperature to decrease with increasing input power. Such a trend was also anticipated in

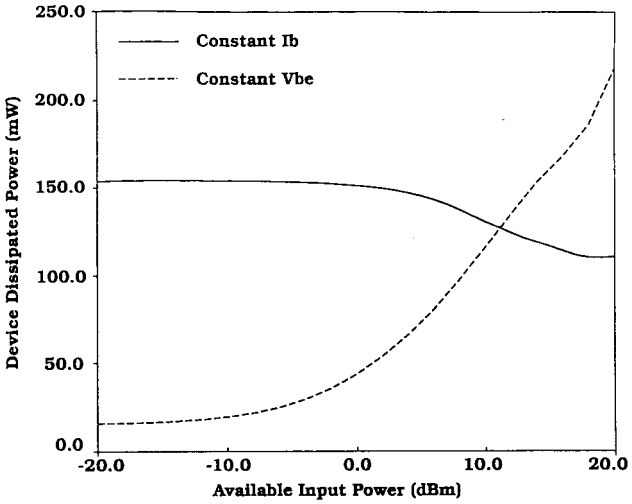

Fig. 8. Device dissipated power dependence on dc bias schemes and RF-excitation levels.

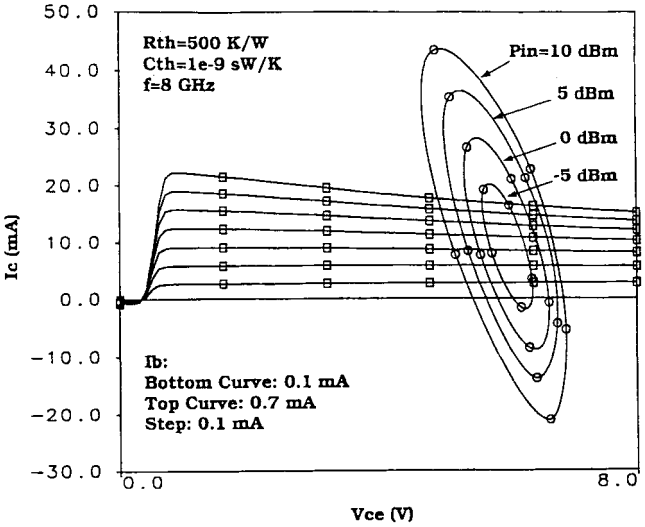

Fig. 9. Simulated load lines of HBT with $R_{\rm th} = 500$ K/W and nonzero $C_{\rm th}$ ($I_B = 0.32$ mA).

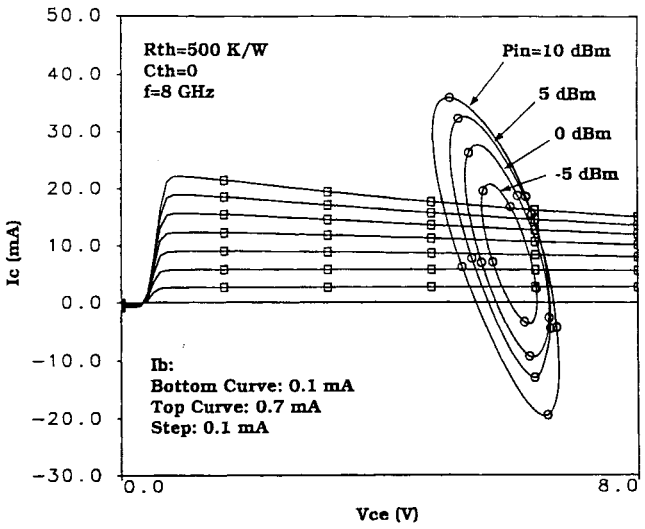

Fig. 10. Simulated load lines of HBT with $R_{\rm th} = 500$ K/W and zero $C_{\rm th}$ ($I_B = 0.32$ mA).

[28] for devices operating under constant I_B bias. Thus, the dependence of PAE on input power dominates over self-bias under constant I_B. The trends for constant $V_{\rm BE}$ are speculated to be opposite to those present under constant I_B. Overall, it appears that while maximum power and efficiency can be achieved at high input power levels using constant $V_{\rm BE}$ bias, self-heating is more pronounced than in the case of constant I_B bias.

Finally, the role of the thermal capacitance on the device large-signal characteristics was also investigated. The thermal sub-circuit considered in the authors' model (Fig. 2) consists of the parallel combination of a resistor and a capacitor. For large thermal capacitance $C_{\rm th}$, values (10^{-9} sW/K) its *RC* time constant is of the order of 0.5 μs which is much higher than the period of the applied RF-signal. The authors will treat this problem by considering the sweep of the output RF-signal through the dc I_C–$V_{\rm CE}$ characteristics for devices with very large or zero thermal capacitance. Although this hypothetical situation corresponds to extreme variations of $C_{\rm th}$ values which are not encountered in practice, it is useful for demonstrating the overall impact of $C_{\rm th}$ on large-signal characteristics of HBT's with different $C_{\rm th}$. During the time that the signal sweeps through the I_C–$V_{\rm CE}$ characteristics, one goes through different I_C, $V_{\rm CE}$ and, therefore, different temperature conditions. One would intuitively expect that for a zero $C_{\rm th}$ system any temperature changes due to different I_C, $V_{\rm CE}$ values will be felt instantaneously by the device. This is not, however, true for large $C_{\rm th}$ values where no temperature variation occurs during signal sweep. The HBT temperature remains, in this case, constant and equal to a value determined by the originally selected bias point and the self-bias, PAE trade-offs discussed earlier. Comparing the operation of devices with large versus small $C_{\rm th}$ values, one can consequently expect that the latter will manifest temperature variations during RF-sweep which could lead to a different range of RF-load line values and, thus, gain and power differences. As will be shown below, this is found to degrade the large-signal performance of HBT's with small $C_{\rm th}$ when constant I_B bias is used.

By way of comparison, the effects of $C_{\rm th}$ on the RF load lines in the case of constant I_B bias conditions ($I_B = 0.32$ mA) are shown in Figs. 9 and 10 for $C_{\rm th} = 10^{-9}$ sW/K and $C_{\rm th} = 0$, respectively. As one observes, the RF-swing at high power levels is larger in the case of large $C_{\rm th}$ values. This is attributed to the fact that, in the zero $C_{\rm th}$ case, the temperature sweeps during part of the RF-cycle through values that are higher than the invariable temperature level corresponding to large $C_{\rm th}$. In the zero $C_{\rm th}$ case, the output signal sweeps through I_c–$V_{\rm ce}$ values that follow the dc I_C–$V_{\rm CE}$ characteristics and are lower than the values swept in the case of large $C_{\rm th}$. Furthermore, the gain at high power levels is by more than 3 dB higher for large $C_{\rm th}$ values. Overall, it appears that presence of thermal capacitance enhances the capability of the device to deliver high output power levels when constant I_B is used for bias.

The above-described characteristics were found to be different for the HBT's of this study in the case of constant

$V_{\rm BE}$ bias. Thermal effects enhance, in this case, the turn-on of the HBT leading to a change of the slope of the dc I_C–$V_{\rm CE}$ characteristics to more positive values. A slightly larger RF-swing was found in this case for zero $C_{\rm th}$ values and as a result enhanced self-bias and self-heating effects will be manifested compared with the large $C_{\rm th}$ case. Further analysis of these effects showed, however, that the gain at high input power levels is the same regardless the value of $C_{\rm th}$ when the constant $V_{\rm BE}$ bias scheme is used.

VI. Conclusion

A Gummel–Poon large-signal model incorporating self-heating effects was employed for the analysis of the microwave power characteristics of HBT's. The model has been implemented in a commercial microwave circuit simulator. The impact of self-heating effects and bias on HBT large-signal performance was studied. RF-excitation was found to reduce self-heating effects on devices biased with a constant I_B. On the other hand, constant $V_{\rm BE}$ bias enhances the ability of HBT's to deliver maximum output power. The HBT thermal capacitance $C_{\rm th}$ was found to be beneficial for large output power operation when constant I_B is used but does not play a significant role in the case where constant $V_{\rm BE}$ bias is employed. Constant $V_{\rm BE}$ bias is more suitable for high-power HBT applications.

References

[1] L. L. Liou, C. I. Huang, and J. Ebel, "Numerical studies of thermal effects on heterojunction bipolar transistor current-voltage characteristics using one-dimensional simulation," *Solid-State Electron.*, vol. 35, no. 4, pp. 579–585, Apr. 1992.

[2] J. J. Liou, L. L. Liou, C. I. Huang, and B. Bayraktaroglu, "A physics-based, analytical heterojunction bipolar transistor model including thermal and high-current effects," *IEEE Trans. Electron Devices*, vol. 40, pp. 1570–1577, Sept. 1993.

[3] L. L. Liou, B. Bayraktaroglu, and C. I. Huang, "Thermal runaway analysis of high power AlGaAs/GaAs heterojunction bipolar transistors," in *IEEE Cornell Conf. 1993 Proc.*, Ithaca, NY, Aug. 1993, pp. 468–477.

[4] B. Bayraktaroglu, R. Fitch, J. Barrette, R. Scherer, L. Kehias, and C. I. Huang, "Design and fabrication of thermally-stable AlGaAs/GaAs microwave power HBT's," in *IEEE Cornell Conf. 1993 Proc.*, Ithaca, NY, Aug. 1993, pp. 83–92.

[5] B. Bayraktaroglu, J. Barrette, L. Kehias, C. I. Huang, R. Fitch, R. Neidhard, and R. Scherer, "Very high-power-density CW operation of GaAs/AlGaAs microwave heterojunction bipolar transistors," *IEEE Electron Device Lett.*, vol. 14, pp. 493–495, Oct. 1993.

[6] L. L. Liou, B. Bayraktaroglu, C. I. Huang, and J. Barrette, "The effect of thermal shunt on the current instability of multiple-emitter-finger heterojunction bipolar transistors," in *IEEE Bipolar Circuits and Technol. Meeting 15-3*, Minneapolis, MN, Oct. 1993, pp. 253–256.

[7] P. Baureis, D. Seitzer, and U. Schaper, "Modeling of self-heating in GaAs/AlGaAs HBT's for accurate circuit and device analysis," in *GaAs-IC Symp. Dig.*, Monterey, CA, Oct. 1991, pp. 125–128.

[8] C. McAndrew, "A complete and consistent electrical/thermal HBT model," in *IEEE 1992 Bipolar Circuits and Technol. Meeting Proc.*, Minneapolis, MN, Oct. 1992, pp. 10.1.1–10.1.4.

[9] Q. M. Zhang, J. Hu, J. Sitch, R. K. Surridge, and J. M. Xu, "A new large-signal HBT model," in *MTT-S Symp. Dig.*, San Diego, CA, May 1994, pp. 1253–1256.

[10] D. S. Whitefield, C. J. Wei, and J. C. M. Hwang, "Temperature-dependent large signal model of heterojunction bipolar transistors," in *GaAs IC Symp.*, Miami Beach, FL, Oct. 1992, pp. 221–224.

[11] K. Lu, P. Perry, and T. J. Brazil, "A new SPICE-type heterojunction bipolar transistor model for dc, microwave small-signal and large-signal circuit simulation," in *MTT-S Symp. Dig*, San Diego, CA, May 1994, pp. 1579–1582.

[12] K. Lu, P. A. Perry, and T. J. Brazil, "A new large-signal AlGaAs/GaAs HBT model including self-heating effects, with corresponding parameter extraction procedure," *IEEE Trans. Microwave Theory Tech.*, vol. 43, pp. 1433–1445, July 1995.

[13] G. Massobrio and P. Antognetti, *Semiconductor Device Modeling with SPICE*, 2nd ed. New York: McGraw-Hill, pp. 45–130, 1993.

[14] A. A. Grinberg, M. S. Shur, R. J. Fischer, and H. Morkoc, "An investigation of the effect of graded layers and tunneling on the performance of AlGaAs/GaAs heterojunction bipolar transistors," *IEEE Trans. Electron Devices*, vol. ED-31, pp. 1758–1765, Dec. 1984.

[15] A. A. Grinberg and S. Luryi, "On the thermionic-diffusion theory of minority transport in heterojunction bipolar transistors," *IEEE Trans. Electron Devices*, vol. 40, pp. 859–866, May 1993.

[16] J. J. Liou, C. S. Ho, L. L. Liou, and C. I. Huang, "An analytical model for current transport in AlGaAs/GaAs abrupt HBT's with a setback layer," *Solid-State Electron.*, vol. 36, no. 6, pp. 819–825, 1993.

[17] J. J. X. Feng, D. L. Pulfrey, J. Sitch, and R. Surridge, "A physics based HBT SPICE model for large-signal applications," *IEEE Trans. Electron Devices*, vol. 42, pp. 8–14, Jan. 1995.

[18] K. Yang, J. C. Cowles, J. R. East, and G. I. Haddad, "Theoretical and experimental dc characterization of InGaAs-based abrupt emitter HBT's," *IEEE Trans. Electron Devices*, vol. 42, p. 1047–1057, June 1995.

[19] M. E. Hafizi, C. R. Crowell, and M. E. Grupen, "The dc characteristics of GaAs/AlGaAs heterojunction bipolar transistors with application to device modeling," *IEEE Trans. Electron Devices*, vol. 37, pp. 2121–2129, Oct. 1990.

[20] P. R. Strickland, "The thermal equivalent circuit of a transistor," *IBM J.*, Jan. 1959, pp. 35–45.

[21] J. R. Waldrop, K. C. Wang, and P. M. Asbeck, "Determination of junction temperature in AlGaAs/GaAs heterojunction bipolar transistors by electrical measurement," *IEEE Trans. Electron Devices*, vol. 39, pp. 1248–1250, May 1992.

[22] G. Gao, S. Unlu, H. Morkoc, and D. L. Blackburn, "Emitter ballasting resistor design for, and current handling capability of AlGaAs/GaAs power heterojunction bipolar transistors," *IEEE Trans. Electron Devices*, vol. 38, pp. 185–196, Feb. 1991.

[23] S. Prasad, Private communication.

[24] H. Kroemer, "Heterostructure bipolar transistors and integrated circuits," *Proc. IEEE*, vol. 70, pp. 13–25, Jan. 1982.

[25] W. I. Wang and F. Stern, "Valence band offset in AlAs/GaAs heterojunctions and the empirical relation for band alignment," *J. Vac. Sci. Technol. B. Microelectron.*, vol. 3, p. 1280–1284, 1985.

[26] A. Samelis, D. R. Pehlke, and D. Pavlidis, "Volterra series based nonlinear simulation of HBT's using analytically extracted models," *Electron. Lett.*, vol. 30, no. 13, pp. 1098–1100, June 23, 1994.

[27] D. R. Pehlke and D. Pavlidis, "Evaluation of the factors determining HBT high-frequency performance by direct analysis of S-parameter data," *IEEE Trans. Microwave Theory Tech.*, vol. 40, pp. 2367–2373, Dec. 1992.

[28] N. L. Wang, N. H. Sheng, M. F. Chang, W. J. Ho, G. J. Sullivan, E. A. Sovero, J. A. Higgins, and P. M. Asbeck, "Ultrahigh power efficiency operation of common-emitter and common-base HBT's at 10 GHz," *IEEE Trans. Microwave Theory Tech.*, vol. 38, pp. 1381–1389, Oct. 1990.

Apostolos Samelis was born in Kalamata, Greece, on November 8, 1967. He received the Diploma in electrical engineering (with distinction) in 1990 from the University of Patras, Greece, and the M.S. and Ph.D. degrees in electrical engineering from the University of Michigan, Ann Arbor, in 1991 and 1996 respectively. His Ph.D. work dealt with the development of bias dependent HBT small-signal equivalent circuit parameter extraction techniques, device design based analysis, and optimization of intermodulation distortion in HBT's, the analysis of thermal effects and breakdown in HBT's using physics-based and circuit-oriented large-signal models, and the investigation of the power, Intermodulation and efficiency trade-offs of power HBT's.

In April 1996, he joined Rockwell Semiconductor Systems, Newbury Park, CA, where he is working on HBT large-signal modeling and characterization.

Dimitris Pavlidis (S'73-M'76-SM'83-F'93) received the B.Sc. degree in physics from the University of Patras, Patras, Greece, in 1972 and the Ph.D. degree from the University of Newcastle, Newcastle-upon-Tyne, U.K., in 1976.

He continued as a Post-Doctoral Fellow at Newcastle until 1978, engaged in work on microwave semiconductor devices and circuits. Since 1986, he has been Professor of Electrical Engineering and Computer Science at the University of Michigan, Ann Arbor. In 1978 he joined the High Frequency Institute of the Technical University of Darmstadt, Germany, working on III–V devices and establishing a new semiconductor technology facility. In 1980 he worked at the Central Electronic Engineering Research Institute, Pilani, India, as UNESCO consultant. From 1980 to 1985, he was Engineer and Manager of the GaAs Monolithic Microwave Integrated Circuits (MMIC) Department of Thomson-CSF, Corbeville, France. Since 1986 he has been involved in research on heterostructure devices and materials at the University of Michigan. His materials research covers InP and Nitride based materials using Metalorganic Chemical Vapor Deposition (MOCVD). His work in the above areas has been reported in numerous papers and reports and he holds six patents.

Prof. Pavlidis was awarded the European Microwave prize for his work in InP-based monolithic integrated HEMT amplifiers in 1990. In 1991, he received the decoration of "Palmes Académiques" in the order of Chevalier by the French Ministry of Education for his work in education. In 1992 he received the Japan Society of Promotion of Science Fellowship for Senior Scientists/Professors from the Japanese Government and the Humbolt Research Award for Distinguished senior U.S. Scientists.